Physics of Fluids

RESEARCH ARTICLE | NOVEMBER 01 2023

Computer modeling of thermotransport in a uniform binary liquid solution with equimolar n-alkane mixtures

Jun Zhong (钟军) ; Shenghua Xu (徐升华)

Check for updates

Physics of Fluids 35, 112004 (2023)
https://doi.org/10.1063/5.0170833

View Online
Export Citation

08 April 2024 04:03:49

AIP Publishing

Physics of Fluids ARTICLE pubs.aip.org/aip/pof

Computer modeling of thermotransport in a uniform binary liquid solution with equimolar n-alkane mixtures

Cite as: Phys. Fluids **35**, 112004 (2023); doi: 10.1063/5.0170833
Submitted: 4 August 2023 · Accepted: 4 October 2023 ·
Published Online: 1 November 2023

View Online Export Citation CrossMark

Jun Zhong (钟军),[1,a)] and Shenghua Xu (徐升华)[2]

AFFILIATIONS

[1]College of Materials Engineering, North China Institute of Aerospace Engineering, Langfang 065000, People's Republic of China
[2]Institute of Mechanics, Chinese Academy of Sciences, Beijing 100190, People's Republic of China

[a)]Author to whom correspondence should be addressed: settings83@hotmail.com

ABSTRACT

By means of molecular dynamics (MD), two novel methods, *a thermal mean-path* that may outline temperature profiles effectively in the MD system and *a modified coarse-grained force field potential* (the MCG-FFP) that may depict inter/intra-molecular interactions fairly well among n-alkane species, are employed to simulate a thermotransport process in a uniform liquid solution with two equimolar n-pentane (nC-5) and n-decane (nC-10) mixtures. In addition, all the MD simulations are running under two constraints: a weak thermal gradient exerting on the MD system from its hot through cold boundary sides and the standard-state acting on the MD system from its outer environment. During the whole MD simulations, coefficients of thermal diffusion and mass mutual diffusion, and the Soret coefficient (SC) for the MD system are calculated by using the MCG-FFP. As a result, the MD simulations indicate that nC-5 species with light molar-mass would migrate toward the hot boundary region, while nC-10 species with heavy molar-mass would migrate toward the cold one. Coefficients calculated from the MCG-FFP are found to meet relevant experimental outputs fairly well. Furthermore, *an empirical formula* developed by means of relevant continuum methods is used for calculating coefficients of mass mutual diffusion in solutions mixing with multimolar nC-5 and nC-10 species. Its one output is found to corroborate pretty well with that from the MD simulations. This may expect that such *the formula* would perform universally when characterizing properties of mass mutual diffusion in binary liquid solutions with other multimolar alkane mixtures in the petroleum engineering.

Published under an exclusive license by AIP Publishing. https://doi.org/10.1063/5.0170833

08 April 2024 04:03:49

I. INTRODUCTION

In the current petroleum engineering, how to delimit a crude oil reservoir effectively underneath should be mainly dependent upon an accurate prediction of distributions for mass fractions from relevant chemical components in the oil reservoir. Early lab works revealed that the Soret effect (the SE), known as an important phenomenon that may have relevant chemical components migrate accordingly during thermotransports which were solely governed by weak thermal gradients from their outer environments, would play a main role in exploring crude oil resources.[1–4] Therefore, several world's class research institutions have focused on the SE studies for over two decades.[1–15] In 2016, according to "the Sino-EU Cooperative Soret Coefficients (SC) in Crude Oil Project," a SJ-10 spacecraft (the SJ-10 Project) carrying six synthesized sample-cells with multicomponent normal-alkane (n-alkane) mixtures was launched into the Space so as to make clear whether the SE did play a sole role in influencing distributions of mass fractions from n-alkane mixtures in crude oils or not, but without an impact of gravitation.[16,17]

Contemporaneously, with the rapid development of computational algorithms, some modeling methodologies such as molecular dynamics (MD), the Monte Carlo (MC), and the Finite Element Method (FEM), etc. have been applied powerfully to investigations of the SE mechanisms for several uniform liquid solutions mixing with various chemical components, and thus worked out some amazing outputs. For examples, Montel and Galliéro[18] applied the MD simulations with different Lennard–Jones (L-J) potentials to the studies of isothermal and non-isothermal properties of some organic liquids. They observed that, in the SE, all the liquid components would migrate diversely. Touzet *et al.*[19] applied the MD simulations with various simple rigid-sphere L-J potentials to a study of a uniform ternary liquid solution mixing with methane (nC-1), n-butane (nC-4), and n-dodecane (nC-12). They also observed that, qualitatively, nC-1 and

Published under an exclusive license by AIP Publishing

nC-4 molecules would migrate toward a hot region in the solution, while nC-12 molecules would migrate toward a cold one. Still in the SJ-10 Project, by means of the Gas Chromatography (GC) and the MD simulations with some simple L-J potentials, Galliéro *et al.*[17,20] investigated the thermodiffusion of methane (nC-1), n-butane (nC-4), and n-dodecane (nC-12) molecules in those six sample-cells. They also observed that, qualitatively, nC-1 and nC-4 molecules would migrate toward the high temperature region, but nC-12 molecules would gather toward the low one. In addition, by using the MD simulations with some simple L-J potentials, Mozaffari *et al.*[21] investigated the SE on a uniform ternary liquid solution mixing equimolarly with n-dodecane, tetra-hydro-naphthalene, and iso-butylbenzene. They calculated quantities of the Soret coefficient (SC) and compared them with experimental data from the SJ-10 Project. However, a big deficiency in their works was that some relevant data in a uniform binary liquid solution mixing with nC-5 and nC-10 species were lost from the SJ-10 spacecraft; thus, their SC quantities could hardly be validated.

Overall, one of important factors to carry out the MD simulations successfully was how to constitute very reliable inter-/intra-molecular potentials for relevant research works. Apparently, all the empirical potentials for organic molecules in above seemed to be pretty simple, and thus can merely offer the few qualitative information during the MD simulations. To surmount this shortcoming, Antoun *et al.*[22] investigated the SE on a uniform binary liquid solution mixing with nC-5 and nC-10 molecules by means of a potential model based upon *the all-atom force field*. In this model, all the inter-/intra-molecular potentials consisted of five terms: radial stretching, angular bending, torsion (spatial geometry deforming), van der Waals', and electrostatic interactions. However, in consequence, it had to cost a large amount of computational resource to fulfill their MD simulations. To simplify calculations of interactions among all the molecular species, a so-called *the anisotropic united-atom* (*AUA*) framework, which chose $-CH_2$, $-CH_3$, and CH_4 as three unified interaction units (hence *the united-atoms*) on an alkane conformation, can be viewed as an effective simplified version to substitute for *the all-atom force field*.[23–35] In practices, for real alkane molecules, both torsion and electrostatic terms in *the AUA* framework were found to play obvious roles merely in those alkane isomers (i.e., i-alkane molecules have both a main carbon trunk and other bigger carbon twigs in each of their conformations). Particularly, the torsion term was found to perform obviously only in i-alkane conformations where bigger carbon twigs hinged.[36,37] However, for those n-alkane molecules just having a main carbon trunk in each of their conformations, above two terms from *the AUA* framework can be ignored.[35] Even if, for those supermacro n-alkane molecules with a main trunk having more than ten methyl groups, adopting *the AUA* model would also increase computational overheads during the MD simulations. Given this drawback, if we ran the MD simulations for some superlarge systems that consisted of hundreds of thousands of supermacro alkane molecules under the very long simulation time (e.g., a quasi-microscopic geometry with hundreds of nanometers in size and a quasi-microscopic second scale with hundreds of millions of the MD time steps), we have to take further coarse-graining operations on *the AUA* framework so as to improve the whole computational efficiency.

Recently, Zhong *et al.*[38] provided three new concise coarse-grained beads for depicting some real conformations of macro n-alkane molecules. In their framework, three conventional unified interaction units in *the AUA* model were extended to three larger ones: $-(CH_2)_2-CH_3$, $-(CH_2)_3-CH_3$, and $-(CH_2)_4-CH_3$. They explained that, under the standard-state, most of supermacro alkane molecules would be under the liquid state, but *the conventional united-atoms* ($-CH_2$, $-CH_3$, and CH_4) were usually under the gaseous state. Therefore, interactions among those supermacro alkane molecules could hardly be represented precisely by *the conventional united-atoms*. However, in the actual petrochemical engineering, under the standard-state, $-(CH_2)_2-CH_3$, $-(CH_2)_3-CH_3$, and $CH_3-(CH_2)_3-CH_3$ types were likely liquefied and mainly regarded as basic debris among those macro alkane species under the liquid state. Also, some research results indicated that such basic debris must have rotated thousands of times during each of translational collisions, so they can approximately be viewed as spherical groups.[39] According to these points, under the liquid state, *the modified united-types* can be represented by means of three larger coarse-grained beads: A1[$-(CH_2)_2-CH_3$], A2 [$-(CH_2)_3-CH_3$], and A3[$CH_3-(CH_2)_3-CH_3$], which may well splice those supermacro alkane molecules (both n-alkane and i-alkane types) by means of their effective combinations. Reference 40 indicated that, not only may such a coarse-graining strategy depict the colloidal stability in the petroleum engineering fairly well, but save more computational resources in relevant MD simulations.

Another key technique to simulate the SE successfully was *the nonequilibrium molecular dynamics* (*the NEMD*) which usually chose an algorithm of heat-flow exchange (the ΔQ: the heat convection between a research system and its outer environment) to fulfill its simulations.[31–36] However, some outputs from *the NEMD* simulations indicated that the SC results usually behaved severe fluctuations even if the ΔQ was very small at the initial stage. Then, such SC quantities would become increasingly stable along with the ΔQ increase. This meant that the ΔQ quantity may have a positive impact on the SC calculations once it rose to a certain high level.[36] Nevertheless, this conclusion was quite doubted because thermal fluctuations due to the heat convection in experimental works usually severely disturb the accuracy of the SC determination no matter whether the ΔQ performed obviously larger or not.[38] Thus, such *NEMD* conclusion needed further corroborating.

In another way, under the continuum media scale, Tang *et al.*[41] investigated characteristics of proposed synthetic jet actuator using both *reduced-order network model* and *computational fluid dynamics* (CFD) simulations. Joshi *et al.*[42] studied the energy consumption of slurry transportation by means of their developed model: *the Eulerian RNG* κ-ε *turbulence*, and so on, all of which focused energy efficiency on various media when these media underwent relevant thermotransport processes.

Therefore, in the work here, by means of the MD simulations with a potential model: *the modified coarse-grained force field potential* (the MCG-FFP) discussed in Sec. II, as one of the extension works in Ref. 40, we applied the MCG-FFP to calculations of coefficients of thermal diffusion and mass mutual diffusion in a uniform binary liquid solution with equimolar nC-5 and nC-10 mixtures when these mixtures underwent a thermotransport process governed by a weak thermal gradient. Also, a method of so-called *the thermal mean-path* (the TMPH) was selected for outlining temperature profiles in the MD system so as to improve the accuracy in above calculations.[43,44] Furthermore, *an empirical formula* was developed by means of relevant continuum methods[45,46] to calculate coefficients of mass mutual

08 April 2024 04:03:49

Published under an exclusive license by AIP Publishing

diffusion in binary liquid solutions with multimolar nC-5 and nC-10 mixtures. As one of expectations, we hope that such research methods will perform obviously better than others discussed in above. That would be a wonderful multiscale work if our goal is achieved. Thus, in the future, we may apply these methods to investigations in the petroleum engineering, and on other relevant novel questions like energy efficiency in Refs. 41 and 42 so as to bridge a gap between atomic discrete objects and macro continuum media.

This article is organized as follows: Sec. II narrates the MD simulation methodologies, Sec. III discusses all the MD simulation outputs, and Sec. IV summarizes the conclusions.

II. METHODOLOGIES

A. Constructions of two coarse-grained conformations

Table I lists some physical parameters for two selected n-alkane molecules in nature. Figure 1 shows a schematic of real structures of two selected n-alkane (nC-5 and nC-10) molecules and their modified geometries spliced by three selected coarse-grained beads (A1, A2, and A3).

During current work here, (1) the first-principle (density functional) calculation[23–29] was employed to optimize the coarse-grained conformations, as shown in Fig. 1, which may enrich the fitting information on constituting the MCG-FFP model, but Ref. 40 and other works did not use it before; (2) two different temperatures (T_h and T_l, $T_h > T_l$) were applied at the left (T_h) and right (T_l) boundary zones in a supercuboid reservoir to perform as two different thermostats. After running the MD simulations for very long MD time steps, both of thermostats would impact on these two boundary zones effectively, so a quasi-steadily thermal gradient may go through the whole reservoir region.[45] Such a constraint may eliminate the thermal noise (due to the heat convection) in *the NEMD* simulations. Thus, two points in above were novel in the work here. Please note, an effect of gravitation onto all the MD simulations here was not considered, and all these MD simulations were carried out under the standard-state (e.g., initial pressure = 1.00 atm, initial T_0 = room temperature = 299K).

TABLE I. Some physical parameters of n-pentane (nC-5) and n-decane (nC-10).[40,48] Reprinted with permission from Zhong *et al.*, "Molecular dynamics simulation of the Soret effect on two binary liquid solutions with equimolar n-alkane mixtures," ACS Omega **7**(1), 518–527 (2022). Copyright 2022 Authors, licensed under a Creative Commons Attribution (CC BY) License.

Species	n-pentane	n-decane
Symbol	nC-5	nC-10
Molecular formula	CH_3–CH_2–CH_2–CH_2–CH_3	CH_3–CH_2–CH_2–CH_2–CH_2–CH_2–CH_2–CH_2–CH_3
Molecular conformation	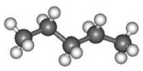	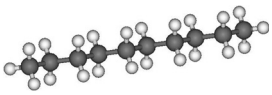
Mass density (g/cm^3, 20 °C)	0.626	0.727
Molar mass (g/mol)	72.18	142.35

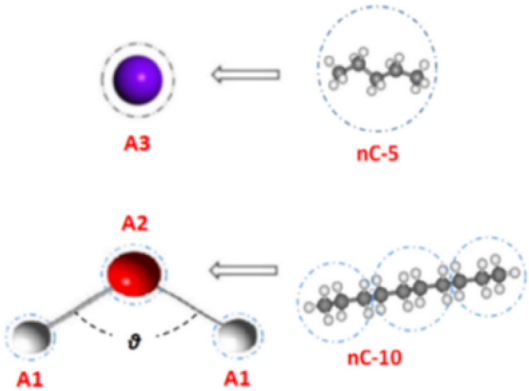

FIG. 1. Coarse-grained modifications for real conformations of two selected n-alkane molecules: nC-5 and nC-10. Reprinted with permission from Zhong *et al.*, "Molecular dynamics simulation of the Soret effect on two binary liquid solutions with equimolar n-alkane mixtures," ACS Omega **7**(1), 518–527 (2022). Copyright 2022 Authors, licensed under a Creative Commons Attribution (CC BY) License.

B. Constitutions of the modified coarse-grained force field potentials

During the MD simulations here, as discussed in Sec. I, both *the AUA* and *the all-atom force field* frameworks usually consisted of two main terms

$$E_{tot} = E_{bond} + E_{nonbond}, \tag{1}$$

where E_{bond} represented strong intra-molecular chemical bonds within one molecular conformation, and $E_{nonradial}$ represented weak inter-molecular interactions among all of molecular species. Then, according to Zhong's work[38] in Sec. I, one nC-5 molecule was modified as an A3 bead only, but one nC-10 molecule was spliced by an A1–A2–A1 chain.

Thus, for each of two electroneutral n-alkane molecules here, Eq. (1) can be simplified as follows:

$$E_{tot} = E_{radial} + E_{angle} + E_{vdw}, \tag{2}$$

where $E_{radial} = k_r\ (r–r_0)^2$, a harmonic model reflecting an effect of radial stretching (k_r was a radial strength, and r_0 was an initial radial quantity); $E_{angle} = k_\vartheta\ (\vartheta - \vartheta_0)^2$, a harmonic model reflecting an effect of angular bending (k_ϑ was an angular strength, and ϑ_0 was an initial angular quantity). Please note, all the k_r, r_0, k_ϑ, and ϑ_0 quantities here were empirical parameters. By means of the DFT calculations,[49,50] the empirical parameters in E_{radial} and E_{angle} terms can be determined through the Birch–Murnaghan Equation of State (BMES) at its harmonic stage.[51,52] Table II lists the fitting parameters for the A1–A2–A1 chain as shown in Fig. 1.

Still coming to Eq. (2), E_{vdw} term was represented by an L-J potential: $E_{vdw} = 4\varepsilon\left[\left(\frac{\sigma}{r}\right)^{12} - \left(\frac{\sigma}{r}\right)^{6}\right]$, where ε and σ were two empirical parameters. Table III lists all the fitting parameters for relevant E_{vdw} terms among A1–A2–A1 and A3 interactions (equivalent to inter-molecular interactions), as shown in Fig. 1. The cutoff distance of the potential tail in each of E_{vdw} terms was chosen as 12.00 Å. Regarding the fitting details, see Ref. 38.

08 April 2024 04:03:49

Published under an exclusive license by AIP Publishing

TABLE II. The fitting parameters for the bonding states in the A1–A2–A1 chain. Reprinted with permission from Zhong *et al.*, "Molecular dynamics simulation of the Soret effect on two binary liquid solutions with equimolar n-alkane mixtures," ACS Omega **7**(1), 518–527 (2022). Copyright 2022 Authors licensed under a Creative Commons Attribution (CC BY) License.

		Bond strength		Bond geometry		
Bead type	Potential term	Radial k_r (eV/Å^2)	Angular k_ϑ (eV/deg^2)	Length r_0 (Å)	Angle ϑ_0 (deg)	Molar-mass of bead (g/mol)
A1–A2–A1	E_{bond}	28.998	0.4129	4.193	179.6	44.107–58.138–44.107
Another calculation[40]		25.911	0.5183	4.180	180.0	–

TABLE III. The fitting parameters to represent van der Waals' interactions among A1, A2, and A3 beads. (Please note: there is no E_{vdw} interactions between A1 and A2 beads within each of molecular conformations). Reprinted with permission from Zhong *et al.*, "Molecular dynamics simulation of the Soret effect on two binary liquid solutions with equimolar *n*-alkane mixtures," ACS Omega **7**(21), 18189 (2022). Copyright 2022 Authors licensed under a Creative Commons Attribution (CC BY) License.

Bead type	Potential term	Bond strength ε (eV)	Bond length σ (Å)	Bead molar mass (g/mol)
A1–A1	E_{vdw}	0.050 69	4.772	44.107–44.107
A1–A2	E_{vdw}	0.056 94	5.012	44.107–58.138
A1–A3	E_{vdw}	0.062 72	5.213	44.107–72.169
A2–A2	E_{vdw}	0.064 36	5.251	58.138–58.138
A2–A3	E_{vdw}	0.071 04	5.452	58.138–72.169
A3–A3	E_{vdw}	0.078 87	5.654	72.169–72.169

TABLE IV. Validations of the MCG-FFP for a uniform binary liquid solution with equimolar nC-5 and nC-10 mixtures.

Index	Calculations	Experiments (Ref. 47)
Mass density (g/cm^3, 20 °C)	0.6764	0.6876
Coefficient of volume thermal expansion ($\times 10^{-3}$, K^{-1})	4.1370	3.8742

Therefore, Eq. (2) can be used for representing the MCG-FFP framework here. Regarding its validations, see some calculation outputs in Table IV.

C. Equation of the thermotransport

In a supercuboid reservoir containing a uniform liquid solution with various mixtures, under an effect of thermal gradient (temperature deference) from its hot through cold boundary sides, mass fractions of mixtures would migrate accordingly.[2–4] Assuming that such a solution just consists of two mixtures (e.g., nC-5 and nC-10 species), thus, a comprehensive flux for component i should obey the following transport law:[2]

$$J_i = -\rho_i D_m^{ij} \nabla C_i - \rho_i D_T C_i(1 - C_i)\nabla T, \tag{3}$$

where T is a thermal temperature acting on the system, C_i is a mass fraction for component i corresponding to the T variable, ρ_i is a mass density for component i, D_T is a coefficient of thermal diffusion, and D_m^{ij} is a coefficient of mass mutual diffusion in the reservoir system. When the system reaches the steady-state (i.e., the $J_i = 0$), both the T and the C_i variables would distribute stationary. Thus, Eq. (1) could be converted as follows:

$$\nabla C_i = -\frac{D_T}{D_m^{ij}} C_i(1 - C_i)\nabla T = -S_T^{ij} C_i(1 - C_i)\nabla T, \tag{4}$$

where $S_T^{ij} = \frac{D_T}{D_m^{ij}}$, defining as the Soret coefficient (SC) for the system, its unit: K^{-1} (generally, its absolute value would represent for its real property). In practices, if the SE is applied to the x-direction only, Eq. (4) will project onto the x-axis as an ordinary differential equation, i.e.,

$$\frac{dC_i}{dx} = -S_T^{ij} C_i(1 - C_i)\left(\frac{dT}{dx}\right). \tag{5}$$

Therefore, along the x-axis, Eq. (5) may usually describe the thermotransport process in most of actual uniform binary liquid solutions. Furthermore, if a weak thermal gradient is exerting on the system (e.g., less than the temperature difference of 10 K, an actual environment around oil reservoirs underneath), all the quantities like C_i, D_T, and D_m^{ij} would perform gently.[46] In this situation, the S_T^{ij} can be viewed as a constant value throughout the whole system region.[46] Thus, along the x-direction, for this system, if applying two hot and cold edge-zones at its left (T_h) and right (T_l) boundary sides ($T_h > T_l$, indicating two different thermostats), and naming C_i^h the mass fraction for component i in the hot edge-zone and C_i^l the one in the cold edge-zone, the S_T^{ij} in Eq. (5) can be modified by means of the finite difference method,[46] i.e.,

$$S_T^{ij} = -\frac{1}{\overline{C}_i(1 - \overline{C}_i)} \cdot \frac{\delta C_i}{\delta T}, \tag{6}$$

where $\overline{C}_i$ represents an average value for component i in the middle region of the system, and $\delta C_i = C_i^h - C_i^l$ and $\delta T = T_h - T_l$, see Ref. 38.

III. SIMULATION PROCEDURES

A. Construction of the MD system

All the MD simulations here were carried out by *the Large-scale Atomic/Molecular Massively Parallel Simulator* (LAMMPS).[53] In initial preparations, the MD system full of 983 040 coarse-grained beads representing for two equimolar A3(nC-5) and A1–A2–A1(nC-10) mixtures was constructed in a supercuboid reservoir, its volume: 1230 × 330 × 330 Å^3 (the quasi-micrometers in length). In the three-dimensional geometric sizes of this MD system, (1) along the x-direction only,

08 April 2024 04:03:49

Published under an exclusive license by AIP Publishing

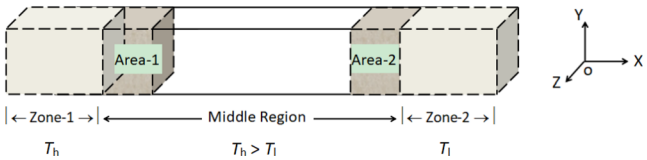

FIG. 2. Geometry of the whole MD system region. Reprinted with permission from Zhong *et al.*, "Molecular dynamics simulation of the Soret effect on two binary liquid solutions with equimolar n-alkane mixtures," ACS Omega **7**(1), 518–527 (2022). Copyright 2022 Authors, licensed under a Creative Commons Attribution (CC BY) license).

two edge-zones (zone-1 and zone-2) were set to 131 Å in lengths respectively, and the middle region comprising with 11 cuboid cells was set to 968 Å in length (each cell length along the x-direction: 88 Å). Inside the middle region, two areas (area-1 and area-2) were adjacent to zone-1 and zone-2, respectively, each of which was set to 176 Å in length. As a result, both nC-5 and nC-10 species numbers moving into these areas and edge-zones could be counted during the thermotransport process. (2) Along the y- and z-directions, two periodic boundary conditions were acting on them respectively, see Fig. 2.

After the geometric construction for the MD system, all the MD simulations were carried out by means of the MCG-FFP discussed in Sec. II B. In addition, along the x-direction, both zone-1 and zone-2 were coupling with two different thermostats (i.e., $T_h = 305$ K for zone-1 and $T_l = 299$ K for zone-2). So the temperature difference between two edge-zones: $\delta T = 6$ K, meeting with the actual environment around oil reservoirs underneath. However, the temperature coupling was not applied to the middle region in Fig. 2, but allowed the heat convection to flow along the x-direction from hot zone-1 to cold zone-2 in this region, which was called *the constant energy (the NVE) MD simulation.*[45] Please note, along the x-direction, two vacuum spaces must be set outside zone-1 and zone-2, respectively, both of their lengths were set to larger than two cutoff distances. Regarding more relevant information on the MD simulations, see Ref. 38.

B. Temperature profiles in the MD system

In this section, temperature profiles in the MD system were outlined for thermal calculations. For example, during the MD simulations, at a selected MD time step (under one MD transient state), a temperature value that may represent the medium effect at site i in the MD system was calculated by the following equation:

$$\frac{3}{2} n\, k_B T_i' = \frac{1}{2} \sum_k m_k \boldsymbol{v}_k^2, \tag{7}$$

where k_B was the Boltzmann constant, T_i' was called *a medium temperature* at site i (actually, a particle's position could be viewed as a medium site in the MD system),[43] m_k and $\boldsymbol{v}_k$ were mass and velocity of particle k, and n was the number of particles inside a sphere with a radius of R at site i. The R was called *the thermal mean-path* (TMPH) which may convert all the kinetic energies of particles inside the sphere i to *the medium temperature value* at site i by using Eq. (7), and so on for other position sites in the MD system.[44] At here, the key manner was how to determine an optimized R quantity effectively. For example, if the MD system was under an equilibrated temperature: T', at one MD time step (also the MD transient state), selecting an initial R value at first, then all *the medium temperatures* corresponding to their position sites inside the MD system can be obtained from Eq. (7). Then, they may acquire a minimum root mean square deviation from the T' value by varying the R value gradually, until an optimized R quantity was well determined. Moreover, such manner was also carried out for other selected MD time steps (other MD transient states) to generate other new optimized R values. Apparently, if the MD system did reach the T' equilibrium, all these optimized R quantities should be deviated least from each other. Finally, all these optimized R quantities corresponding to their MD time steps must take an arithmetic-mean one, which was called *the optimized ensemble-mean value*. Thus, according to this manner, the finally optimized R mean value in the work here was determined as 88 Å, corresponding to a temperature range of [299, 305] K. Based upon this value, temperate profiles in the MD system could be well outlined.

C. Coefficients of thermal diffusion and mass mutual diffusion

In a uniform binary liquid solution (an isotropic system), by means of Eq. (3), both thermal diffusion and mass mutual diffusion along the x-direction should obey the Fick's law.[2] Such a phenomenological equation can be expressed as follows:

$$\frac{\partial u}{\partial t} = D_u \frac{\partial^2 u}{\partial x^2}, \tag{8}$$

where t was the MD simulation time (also the diffusion time), u denoted the T or the C_i variable in the system, and D_u represented a relevant diffusion coefficient for the u index. If setting u_h and u_l to represent relevant quantities in respective hot edge-zone (zone-1) and cold edge-zone (zone-2) in Fig. 2, the solution of Eq. (8) could be expressed as follows:[46]

$$\frac{u(x) - u_l}{u_h - u_l} = 1 - \boldsymbol{erf}(\beta), \tag{9a}$$

where *the* $\boldsymbol{erf}(\beta)$ *function* was called *the Gaussian error function*, in which

$$\beta = \frac{x}{2 \cdot \sqrt{D_u \cdot t}}. \tag{9b}$$

Based upon Eqs. (9a) and 9(b), the T solution can expressed as follows:

$$T(x) = T_l + \delta T \cdot [1 - \boldsymbol{erf}(\beta)], \tag{10a}$$

where δT was a temperature driving force (here, $\delta T = 305 - 299 = 6$ K), and T_l was the temperature applied onto the cold edge-zone (zone-2). Also, Eq. (10a) can be modified as follows:

$$dT = T(x) - T_l = \delta T \cdot [1 - \boldsymbol{erf}(\beta)]. \tag{10b}$$

Since the geometry of the MD system here was near micrometers in size, it may ignore an effect of phonon ballistic transport during the MD simulations.[54]

1. Coefficient of thermal diffusion (D_T)

Here, the D_T can be calculated by means of Eqs. (9) and (10) and the method in Sec. III B. In specific details, (1) within the middle

08 April 2024 04:03:49

Published under an exclusive license by AIP Publishing

region in Fig. 2, 44 slices with an adjacent spacing of 22 Å were chosen to be perpendicular to the x-axis, each of which must delimit a ± 11 Å scope around the x-coordinate of its central point: x_i. As a result, 44 adjacent thin blocks were constructed along the x-direction so as to receive more precise T quantities in calculations. (2) At one selected MD time step, for example, in a thin block i, all *the medium temperatures* within this block scope were summarized to achieve an arithmetic-mean one: $\overline{T}(x_i)$. In fact, this step was identical to taking an arithmetic-mean quantity from several measuring data for a testing variable in the experimental work. Other thin blocks may obtain their respective $\overline{T}(x_i)$ values by using this method. As a result, one $T'(x)$ spectrum can be outlined by means of these $\overline{T}(x_i)$ values, which was corresponding to that selected MD time step. (3) Then, during the whole MD simulations, several MD time intervals (several different δt values) were selected to show up their new optimized $T(x, \delta t)$ curves, for example, for one selected δt value, it should contain hundreds of million MD time steps. Thus, during this time interval, 500 favorite $T'(x)$ spectrum (corresponding to 500 selected MD time steps) were collected to optimize a new $T(x, \delta t)$ curve for the δt. Then, such a manner was used for obtaining other new $T(x, \delta t)$ curves corresponding to their own δt values. The main purpose of this work was to verify whether these new optimized $T(x, \delta t)$ curves would distribute steadily or not. (4) Finally, an optimized D_T value can be determined by means of these optimized $T(x, \delta t)$ curves.

2. Coefficient of mass mutual diffusion (D_m^{ij})

Some monographs narrated that[55,56] if a binary liquid solution was under a thermal impact from its outer environment, the coefficient of mass mutual diffusion (the D_m^{ij}) in this system would be fairly sensitive to this impact even if it would perform merely a weak alteration. As a result, the D_m^{ij} quantity would be very hard to measure in high accuracy under such thermal influences.

Alternatively, according to the SC definition, $S_T^{ij} = \frac{D_T}{D_m^{ij}}$, the D_m^{ij} quantity could be determined by means of this definition. In addition, by referring the main contributions in relevant monographs,[56–58] here we developed *a universal empirical formula* based upon thermodynamics, which was very valuable for depicting the D_m^{ij} quantities in uniform binary liquid solutions with multimolar n-alkane mixtures when they were under a weak thermal impact from their outer environments, i.e.,

$$D_m^{ij} = 2.628 \times \frac{\sqrt{(T^*)^3 \cdot \left(\frac{x_i}{M_i} + \frac{x_j}{M_j}\right)^{\alpha}}}{p_{atm} \cdot \left(l_{ij}^*\right)^2 \cdot \Omega_D}. \tag{11}$$

To make the D_m^{ij} calculation more feasible, here we did not convert all the variable units in Eq. (11) to the SI ones, but still followed a scientific custom by which researchers may directly substitute significant digits of variables into Eq. (11) to finish the calculation. Thus, in this case, α was a power index (no unit); p_{atm} was a relative pressure, its unit: atm; $T^* = k_B \cdot T_{eff}/\varepsilon_{ij}^*$, a reduced temperature (no unit) in the middle region of the MD system (T_{eff} was an effective medium temperature in the middle region, which was influenced by two boundary temperatures: T_h and T_l, its unit: K); k_B was the Boltzmann constant, its unit: $\frac{1}{11\,604.5} \cdot \frac{\text{eV}}{\text{K}}$; and ε_{ij}^* was an effective bond strength between i and j molecules, its unit: eV. Also, M_i and M_j were molar-masses for two different molecules i and j, their units: g/mole; x_i and x_j were molar fractions for two different molecules i and j (here $x_i + x_j = 1.00$); l_{ij}^* was an arithmetic-mean value from two different molecular chain-lengths: $l_{ij}^* = \frac{1}{2}(l_i + l_j)$, its unit: Å; and Ω_D was called *the transport function* (no unit),[57,58] which was a function of the T^* variable. Finally, the unit of the D_m^{ij} variable: cm^2/s.

Apparently, Eq. (11) held the relevant information of atomic objects (e.g., l_{ij}^*, x_i, and x_j, and M_i and M_j) and the continuum media (e.g., T^*, Ω_D, and p_{atm}), which may well represent a multiscale property here, and thus can be employed to corroborate with the output from the MD simulations.

IV. RESULTS AND DISCUSSION

A. Reexamining the Soret coefficient

Figure 3 shows distributions for mass fractions of nC-5 and nC-10 species along the x-direction in the MD system corresponding to $\delta T = T_h - T_l = 6$ K from hot and cold edge-zones (in this figure, such two edge-zones were confined between vertical dashed-lines and boundary sides, respectively). In Fig. 3, during 460 000 000 MD time steps, two curves of mass fractions in the middle region looked flat. However, they would behave different trends during two respective edge-zones, meaning that more nC-5 molecules (with light molar-mass) would migrate toward the hot edge-zone (zone-1) than the cold one (zone-2). Whereas more nC-10 molecules (with heavy molar-mass) would migrate oppositely. These phenomena were also observed in some experimental works.[59–62] Regarding relevant mechanisms, see Ref. 38.

By using Eq. (6), here, the SC quantity (absolute value) in the MD system corresponding to $\delta T = 6$ K was calculated to examine the reliability of the equation. So in this equation, two arithmetic-mean values of mass fractions: $\overline{C}_5$ and $\overline{C}_{10}$ in the middle region were calculated as 0.335 86 and 0.664 14,[38] $T_l = 299$ K was taken as a reference point, and those C_i^h and C_i^l quantities in respective area-1, area-2, zone-1, and zone-2 in Fig. 2 were collected for the SC calculation by means of *the optimized interpolation*.[58] Table V lists the calculated SC output (absolute value).

In two experimental works, quantitatively, Perronace *et al.*[28] reported that in a temperature range from 298 to 302 K ($\delta T = 4$ K) with an average temperature value of 300 K, the SC quantity (absolute value) for a uniform binary liquid solution with equimolar nC5 and nC10 mixtures: $(3.27 \pm 0.23) \times 10^{-3}$ K^{-1}. Also, in a temperature range

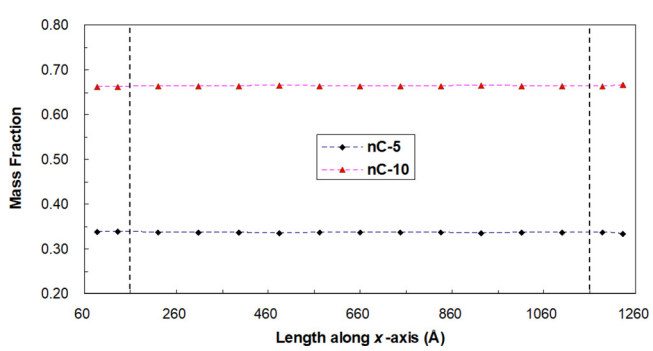

FIG. 3. Distributions for mass fractions of nC-5 and nC-10 species along the x-direction in response to $\delta T = 6$K.

08 April 2024 04:03:49

Published under an exclusive license by AIP Publishing

TABLE V. The SC quantity (absolute value) for the MD system [nC-5⊕nC-10] corresponding to $\delta T = 6$ K ($T_h = 305$ K for hot zone-1 and $T_l = 299$ K for cold zone-2).

Temperatures	hot zone-1 ($T_h = 305$ K)	cold zone-2 ($T_l = 299$ K)
the Soret coefficient, S_T^{ij} ($\times 10^{-3}$, K^{-1})	2.62 ± 0.42	

of $\delta T = 5$ K with an average temperature value of 298 K, de Mezquia *et al.*[47] reported that the SC quantity for this system was $(2.96 \pm 0.11) \times 10^{-3}$ K^{-1}. Thus, comparing with these two results, the SC quantity obtained here: $(2.62 \pm 0.42) \times 10^{-3}$ K^{-1}, in a temperature range of $\delta T = 6$ K with an average temperature value of 302 K, would align with the trend of the SC variable vs the δT span fairly well. Some other experimental works[59–62] reported that an expression of the SC quantity (absolute value) for an isotopic fractional element (e.g., the melting silicate) under a weak thermal gradient would show a function of the inverse of the absolute temperature, i.e., the SC quantity would decline gradually along with the δT increase. Therefore, the SC quantity obtained from the MD simulations here may corroborate what those experimental works observed. So Eq. (6) may be more practical than that in Ref. 38.

B. Calculations of coefficients of thermal diffusion and mass mutual diffusion

1. Coefficient of thermal diffusion

Figure 4 shows the distribution of a selected $T(x, \delta t)$ curve corresponding to a selected MD time interval: (1.00–4.00)·u$_0$, along the x-direction throughout the whole middle region in Fig. 2 (here, $\delta t = 3.00 \cdot$u$_0$, u$_0 = 10^{-7}$ s). During this time interval, in detail, 500 favorite $T'(x)$ spectrum corresponding to their own 500 MD time steps (transient states) were collected to optimize a new $T(x, \delta t)$ curve.

In Fig. 4, along the x-direction, a negative curve tail on the $T(x, \delta t)$ curve (below the zero temperature line) indicated a supercooling effect because of very short MD time steps during the MD simulations. And, an intersecting point of the $T(x, \delta t)$ curve with the x-axis: x_0, was regarded as the positive end of $T(x, \delta t)$ curve contribution for the MD system. Apparently, when $\delta t \to \infty$, the x_0 would tend to a lager stationary value, and the negative curve tail would merge into the zero temperature line, implying that such a supercooling effect would vanish. Thus, the x_0 point here can be used for the D_T calculation by Eq. (9b).

In principle, *the* ***erf***(β) *function* in Eq. (10) has a definite relationship with *the normal distribution function*: $\boldsymbol{\Phi}(z)$, i.e., $\boldsymbol{\Phi}(z) = \frac{1}{2} + \frac{1}{2} erf\left(\frac{z}{\sqrt{2}}\right)$, and $\beta = \frac{z}{\sqrt{2}}$. Usually, there is a so-called $z_m = \pm 6 \cdot \sigma$ scope

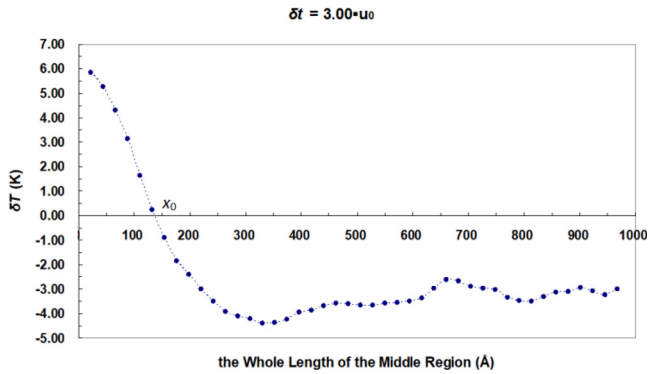

FIG. 4. The $T(x, \delta T)$ curve distribution corresponding to a MD time interval: (1.00–4.00)·u$_0$, $\delta t = 3.00 \cdot$u$_0$, throughout the whole middle region (here, u$_0 = 10^{-7}$ s).

in *the* $\Phi(z)$ *function* (here, σ was reduced to 1.00 as the standard state), within which most of the positive contribution in *the* $\boldsymbol{\Phi}(z)$ function should lay in this optimized region.[63] However, here, since the significant value of the D_T variable was on the order of 10^{-13}, to meet the double precision in computations by using Eq. (9b), such an optimized region should extend to $z_m = \pm 6.109\,41$. As a result, $\beta_m = \frac{z_m}{\sqrt{2}} = 4.320\,01$. Table VI lists some selected x_0 values and their corresponding MD time intervals (each of which started from 1.00·u$_0$, u$_0 = 10^{-7}$ s), plus the calculated outputs of the D_T variable when substituting relevant x_0 and δt values and $\beta_m = 4.320\,01$ into Eq. (9b).

From Table VI, it can be seen that, for those selected MD time intervals, their corresponding x_0 values would hover near 133 Å even if they showed some oscillations around this quantity. As a result, by using Eq. (9b), a finally optimized output of the D_T variable for the liquid solution here was estimated as $(8.900 \pm 0.691) \times 10^{-12}$ m^2·K^{-1}·s^{-1}, in a temperature range of $\delta T = 6$ K (from 299 to 305 K) with an average temperature value of 302 K.

Still coming back to those two experimental works in above, Perronace *et al.*[28] reported that in a temperature range from 298 to 302 K ($\delta T = 4$ K) with an average temperature value of 300 K, the D_T value for the solution in above was $(7.54 \pm 0.61) \times 10^{-12}$ m^2·K^{-1}·s^{-1}. Also, in a temperature range of $\delta T = 5$ K with an average temperature value of 298 K, de Mezquia *et al.*[47] reported that the D_T value for such a system was $(8.76 \pm 0.12) \times 10^{-12}$ m^2·K^{-1}·s^{-1}. So comparing with their results, the D_T value obtained here, $(8.900 \pm 0.691) \times 10^{-12}$ m^2·K^{-1}·s^{-1}, would align with the trend of the D_T variable vs the δT span, i.e., the higher the δT value performed, the higher the D_T quantity would become.

Furthermore, under $\delta T = 6$ K, *the Fluent Simulation Package* based upon *the Finite Element Method* (FEM)[58] was implemented to calculate a thermal conductivity for the liquid solution in above. Some

TABLE VI. Selected x_0 values and their corresponding MD time intervals, plus the calculated D_T values.

Selected MD time intervals, δt($\times$u$_0$)	2.20	2.40	2.60	2.80	3.00	3.20	3.40	3.60
Intercept points, x_0($\times 10^2$ Å)	1.204 33	1.482 13	1.473 49	1.333 14	1.362 01	1.318 38	1.288 50	1.330 90
Coefficient of thermal diffusion, D_T ($\times 10^{-12}$ m^2·K^{-1}·s^{-1})	8.8316	12.2612	11.1865	8.5029	8.2834	7.2762	6.5413	6.5911

08 April 2024 04:03:49

Published under an exclusive license by AIP Publishing

TABLE VII. Comparisons of several D_m^{ij} values corresponding to relevant experimental results. (unit: $\times 10^{-9}$ m^2·s^{-1}, x_i was for nC-5, x_j was for nC-10, and $x_i + x_j = 1.00$).

Molar fraction, x_j		0.100	0.200	0.340	0.500	0.640	0.800
The D_m^{ij} quantity from Eq. (11), $\delta T = 6$K	$\alpha = 2.00$	4.29 ± 0.06	4.07 ± 0.06	3.76 ± 0.06	3.40 ± 0.05	3.09 ± 0.05	2.73 ± 0.04
	$\alpha = 2.02$	4.11 ± 0.06	3.89 ± 0.06	3.59 ± 0.05	3.25 ± 0.05	2.95 ± 0.04	2.61 ± 0.04
	$\alpha = 2.03$	4.02 ± 0.06	3.81 ± 0.06	3.51 ± 0.05	3.18 ± 0.05	2.88 ± 0.04	2.54 ± 0.04
	$\alpha = 2.04$	3.94 ± 0.06	3.73 ± 0.06	3.44 ± 0.05	3.11 ± 0.05	2.82 ± 0.04	2.49 ± 0.04
Experimental data,[a] $\delta T = 5$K		3.75	3.36	3.03	2.86	2.48	2.20

[a]Reference 47.

of input information on such calculation came from Table III, its final output: (0.126 ± 0.003) W·m^{-1}·K^{-1}. In addition, Ref. 28 gave its relevant output under $\delta T = 4$ K: (0.109 ± 0.002) W·m^{-1}·K^{-1}. Therefore, the comparability of these two outputs may support that the MCG-FFP model developed here should be competent for the MD simulations.

2. Coefficient of mass mutual diffusion

According to the SC definition, $S_T^{ij} = \frac{D_T}{D_m^{ij}}$, by means of relevant quantities in Sec. III, the D_m^{ij} value for the solution in above can be determined as (3.40 ± 0.43) × 10^{-9} m^2·s^{-1}. Perronace *et al.*[28] reported that, in a temperature range of 298–302 K with an average temperature value of 300 K ($\delta T = 4$ K), the D_m^{ij} value for this solution was (2.30 ± 0.18) × 10^{-9} m^2·s^{-1}. Also, in a temperature range of $\delta T = 5$ K with an average temperature value of 298 K, de Mezquia *et al.*[47] reported that the D_m^{ij} value for such solution: (2.86 ± 0.10) × 10^{-9} m^2·s^{-1}. So comparing with these results, the D_m^{ij} value obtained here (under $\delta T = 6$ K) would align with the trend of the D_m^{ij} variable vs the δT span, i.e., the higher the δT value behaved, the larger the D_m^{ij} value would become.

Moreover, by means of Eq. (11), here we calculated the D_m^{ij} value to validate with the output from the MD simulations. In detail, for the liquid solution in above, some of parameters in Eq. (11) were determined as follows: Regarding the ε_{ij}^* quantities, considering two ideal cases: (1) two coarse-grained nC-5 and nC-10 species were aligned in parallel, thus $\varepsilon_{ij}^* = \sqrt[6]{(\varepsilon_{A1} \cdot \varepsilon_{A3}) \cdot (\varepsilon_{A2} \cdot \varepsilon_{A3}) \cdot (\varepsilon_{A1} \cdot \varepsilon_{A3})} = 0.065\,80$ eV; (2) such two coarse-grained species were aligned in series, thus $\varepsilon_{ij}^* = \sqrt{(\varepsilon_{A1} \cdot \varepsilon_{A3})} = 0.063\,23$ eV. So among their actual interactions, $\varepsilon_{ij}^* \in [0.063\,23, 0.065\,80]$ eV. Here, M_i and M_j came from Table I, $p_{atm} = 1.00$ atm, $l_{ij}^* = \frac{1}{2}(5.654 + 13.158) = 9.406$ Å, and $\Omega_D \in [2.2869, 2.332]$. Also in the middle region, since $T_{eff} \in [299, 305]$ K, then $T^* \in [0.3955, 0.4116]$.

By taking the combination algorithm for the D_m^{ij} calculations in above, here we determined several D_m^{ij} quantities by means of Eq. (11). In detail, it was found that, when $\alpha = 2.00 \pm \delta$ (δ was a very small correction value), the D_m^{ij} span obtained from Eq. (11) may fit pretty well to that in Ref. 47. According to this finding, some α trial quantities: 2.00, 2.02, 2.03, and 2.04 were selected to observe which of the D_m^{ij} spans obtained from Eq. (11) would align in parallel best with that in Ref. 47. Table VII lists several D_m^{ij} quantities calculated from Eq. (11) corresponding to various x_i and x_j molar fractions in binary liquid solutions with multimolar nC-5 and nC-10 mixtures (here $x_i + x_j = 1.00$, i = nC-5 and j = nC-10). From this table, it can be seen that, when $\alpha = 2.00$, at $x_i = x_j = 0.50$, the D_m^{ij} value was (3.40 ± 0.05) × 10^{-9} m^2·s^{-1}, in a very good agreement with the MD output in above: (3.40 ± 0.43) × 10^{-9} m^2·s^{-1}.

Moreover, when $\alpha = 2.03$, the D_m^{ij} span obtained from Eq. (11) would be the best to align in parallel with that in Ref. 47; see solid- and dotted-lines in Fig. 5. Therefore, here the favorite selection for α was 2.03, and Eq. (11) would become

$$D_m^{ij} = 2.628 \times \frac{\sqrt{(T^*)^3 \cdot \left(\frac{x_i}{M_i} + \frac{x_j}{M_j}\right)^{2.03}}}{p_{atm} \cdot (l_{ij}^*)^2 \cdot \Omega_D}. \tag{12}$$

In addition, when $\alpha = 2.03$, at $x_i = x_j = 0.50$, the D_m^{ij} value obtained from Eq. (12) was (3.18 ± 0.05) × 10^{-9} m^2·s^{-1}, still meeting well with the MD output in above.

Figure 5 shows relevant D_m^{ij} span data obtained from Table VII. A dashed-line curve in this figure denoted the D_m^{ij} span from the experimental work.[47] Through this figure, it may observe that the D_m^{ij} spans obtained from Eq. (11) would show negatively linear relationships with the molar fraction of nC-10 species. Also, de Mezquia *et al.*[47] and Leaty-Dios and Firoozabadi[64] reported that both coefficients of mass mutual diffusion and thermal diffusion would vary same relationships in above with mass fractions in relevant liquid solutions mixing with multimolar n-alkane species, i.e., the variation of the mass fraction was strongly identical to the molar fraction of nC-10 species in Fig. 5. Therefore, Eq. (11) would be very valuable for depicting properties of mass mutual diffusion in those solutions with multimolar nC-5 and nC-10 mixtures under weak thermal impacts from their

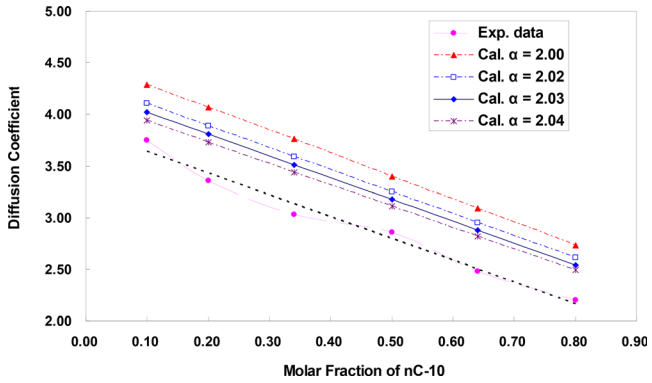

FIG. 5. Comparisons of the calculated D_m^{ij} spans with experimental results.

08 April 2024 04:03:49

Published under an exclusive license by AIP Publishing

outer environments. As an expectation, we hope that *the empirical formula* ([Eq. (11)] developed here would represent properties of mass mutual diffusion universally in binary liquid solutions full of other multimolar alkane mixtures in the petroleum engineering.

V. CONCLUSIONS

In this article, molecular dynamics (MD) was fulfilled to simulate a thermotransport process in a uniform binary liquid solution with equimolar n-pentane (nC-5) and n-decane (nC-10) mixtures. Throughout the whole MD simulations, some conclusions can be drawn as follows:

First, during the MD simulations, *the modified coarse-grained force field potential* (the MCG-FFP) was found to perform very well in calculating thermal properties such as the Soret coefficient and coefficients of thermal diffusion and mass mutual diffusion under a weak thermal impact on the MD system from its outer environment.

Second, *the thermal mean-path* was employed to outline temperature profiles in the MD system so as to improve the accuracy in calculating coefficients of thermal diffusion and mass mutual diffusion. These outputs were found to be in very good agreements with relevant experimental results.

Third, the MD simulations showed that nC-5 species with light molar-mass would migrate toward the high temperature region, while nC-10 species with heavy molar-masses would migrate toward the low temperature region, both of which were observed in relevant experimental works. The modified formula for the SC calculation was found to perform very well.

Finally, an empirical formula developed here showed to represent properties of mass mutual diffusion pretty well in binary liquid solutions mixing with multimolar nC-5 and nC-10 species. This may support our an expectation that, in the future, such *an empirical formula* may play a universal role in the petroleum engineering.

ACKNOWLEDGMENTS

This work was sponsored by the National Science Foundation, USA (Grant No. DMR9619353), the National Natural Science Foundation of China (Grant No. U1738108), and the Hebei Provincial Key Laboratory of Thermal Protection Materials, China (Grant No. SZX2020038). Authors also appreciated Mr. Jinming Wang, Ms. Yifang Cui, and Ms. Ziyi Guo for their valuable efforts on this work.

AUTHOR DECLARATIONS

Conflict of Interest

The authors have no conflicts to disclose.

Author Contributions

Jun Zhong: Data curation (lead); Formal analysis (lead); Funding acquisition (supporting); Investigation (lead); Methodology (lead); Project administration (equal); Resources (equal); Software (lead); Supervision (equal); Validation (lead); Visualization (lead); Writing – original draft (lead); Writing – review & editing (equal). **Shenghua Xu:** Conceptualization (lead); Funding acquisition (lead); Project administration (equal); Resources (equal); Supervision (equal); Writing – review & editing (equal).

DATA AVAILABILITY

The data that support the findings of this study are available from the corresponding author upon reasonable request.

REFERENCES

[1]B. D. Butler and J. C. R. Turner, "Flow-cell studies of thermal diffusion in liquids. Part I. Cell construction and calibration," Trans. Faraday Soc. **62**, 3114–3120 (1966).
[2]F. H. Horne and R. J. Bearman, "Thermogravitational thermal diffusion in liquids. Part I. The formal theory," J. Chem. Phys. **37**(12), 2842–2857 (1962).
[3]F. H. Horne and R. J. Bearman, "Thermogravitational thermal diffusion in liquids. Part II. Experimental thermal diffusion factors for carbon tetrachloride cyclohexane at 25 °C," J. Chem. Phys. **37**(12), 2857–2871 (1962).
[4]M. Giglio and A. Vendramini, "Thermal-diffusion measurements near a consolute critical point," Phys. Rev. Lett. **34**(10), 561–564 (1975).
[5]M. Farber and W. F. Libby, "Effect of gravitational field on the thermal diffusion separation method," J. Chem. Phys. **8**(12), 965–969 (1940).
[6]S. R. de Groot and P. Mazur, *Nonequilibrium Thermodynamics* (Dover Publication Inc., New York, 1953).
[7]C. J. Danby, J. D. Lamber, and C. M. Mitchell, "Separation of hydrocarbon isomers by thermal diffusion," Nature **177**, 1225–1226 (1956).
[8]P. Kolodner, H. Williams, and C. Moe, "Optical measurement of the Soret coefficient of ethanol/water solutions," J. Chem. Phys. **88**(10), 6512–6524 (1988).
[9]F. Montel, "Importance de la thermodiffusion en exploration et production pétrolières," Entropie **30**(184–185), 86–93 (1994).
[10]K. J. Zhang, M. E. Briggs, and R. W. Gammon, "Optical measurement of the Soret coefficient and the diffusion coefficient of liquid mixtures," J. Chem. Phys. **104**(17), 6881–6892 (1996).
[11]L. Hùier and C. H. Whitson, "Compositional grading—Theory and practice," SPE Reservoir Eval. Eng. **4**(6), 525–535 (2001).
[12]K. Ghorayeb, A. Firoozabadi, and T. Anraku, "Interpretation of the unusual fluid distribution in the Yufutsu gas-condensate field," SPE J. **8**(2), 114–123 (2003).
[13]J. K. Platten, "The Soret effect: A review of recent experimental results," J. Appl. Mech. **73**(1), 5–15 (2006).
[14]F. Montel, J. Bickert, and A. Lagisquet, "Initial state of petroleum reservoirs: A comprehensive approach," J. Pet. Sci. Eng. **58**(3–4), 391–402 (2007).
[15]M. A. Rahman and M. Z. Saghir, "Thermodiffusion or Soret effect: Historical review," Int. J. Heat Mass Transfer **73**, 693–705 (2014).
[16]W. Hu and Q. Kang, *Physical Science Under Microgravity: Experiments on Board the SJ-10 Recoverable Satellite* (Springer Science Press, Beijing, 2019).
[17]G. Galliéro, H. Bataller, J. Bazile, J. Diaz, F. Croccolo, H. Hoang, R. Vermorel, P. Artola, B. Rousseau, V. Vesovic, M. M. Bou-Ali, J. M. O. d. Zárate, S. Xu, K. Zhang, F. Montel, A. Verga, and O. Minster, "Thermodiffusion in multicomponent *n*-alkane mixtures," npj Microgravity **3**(20), 20 (2017).
[18]F. Montel and G. Galliéro, "Non-isothermal gravitational segregation by molecular dynamics simulations," Phys. Rev. E **78**(4), 041203 (2008).
[19]M. Touzet, G. Galliéro, and V. Lazzeri, "Thermodiffusion: From microgravity experiments to the initial state of petroleum reservoirs," C. R. Mec. **339**(5), 318–323 (2011).
[20]G. Galliéro, H. Bataller, and F. Croccolo, "Impact of thermodiffusion on the initial vertical distribution of species in hydrocarbon reservoirs," Microgravity Sci. Technol. **28**(2), 79–86 (2016).
[21]S. H. Mozaffari, S. Srinivasan, and M. Z. Saghir, "A study on thermodiffusion in ternary liquid mixtures using enhanced molecular dynamics algorithm with experimental validation," Can. J. Chem. Eng. **97**(1), 344–2350 (2019).
[22]S. Antoun, M. Z. Saghir, and S. Srinivasan, "An improved molecular dynamics algorithm to study thermodiffusion in binary hydrocarbon mixtures," J. Chem. Phys. **148**(10), 104507 (2018).
[23]S. Toxvaerd, "Molecular dynamics calculation of the equation of state of alkanes," J. Chem. Phys. **93**(6), 4290–4295 (1990).
[24]P. Padilla and S. Toxvaerd, "Self-diffusion in n-alkane fluid models," J. Chem. Phys. **94**(8), 5650–5664 (1991).
[25]S. Toxvaerd, "Equation of state of alkanes II," J. Chem. Phys. **107**(13), 5197–5204 (1997).

08 April 2024 04:03:49

Published under an exclusive license by AIP Publishing

[26]D. K. Dysthe, A. H. Fuchs, and B. Rousseau, "Fluid transport properties by equilibrium molecular dynamics. I. Methodology at extreme fluid states," J. Chem. Phys. **110**(8), 4047–4059 (1999); "Fluid transport properties by equilibrium molecular dynamics. II. Multicomponent systems," **110**(8), 4060–4067 (1999); "Fluid transport properties by equilibrium molecular dynamics. III. Evaluation of united atom interaction potential models for pure alkanes," **112**(17), 7581–7590 (2000).
[27]P. Ungerer, "Optimization of the anisotropic united atoms intermolecular potential for n-alkanes," J. Chem. Phys. **112**(12), 5499–5510 (2000).
[28]A. Perronace, C. Leppla, F. Leroy, B. Rousseau, and S. Wiegand, "Soret and mass diffusion measurements and molecular dynamics simulations of n-pentane and n-decane mixtures," J. Chem. Phys. **116**(9), 3718–3729 (2002).
[29]Y. Boutard, P. Ungerer, J. M. Teuler, M. G. Ahunbay, S. F. Sabater, A. D. Mackie, J. Pérez-Pellitero, and E. Bourasseau, "Extension of the anisotropic united atoms intermolecular potential to amines, amides and alkanols: Application to the problems of the 2004 fluid simulation challenge," Fluid Phase Equilib. **236**(1–2), 25–41 (2005).
[30]C. Nieto-Draghi, A. Bocahut, B. Creton, P. Have, A. Ghoufi, A. Wender, A. Boutin, B. Rousseau, and L. Normanda, "Optimization of the dynamical behaviour of the anisotropic united atom model of branched alkanes: Application to the molecular simulation of fuel gasoline," Mol. Simul. **34**(2), 211–230 (2008).
[31]W. Allen and R. L. Rowley, "Predicting the viscosity of alkanes using nonequilibrium molecular dynamics: Evaluation of intermolecular potential models," J. Chem. Phys. **106**(24), 10273–10281 (1997).
[32]C. Nieto-Draghi, J. B. Ávalos, and B. Rousseau, "Computing the Soret coefficient in aqueous mixtures using boundary driven nonequilibrium molecular dynamics," J. Chem. Phys. **122**(11), 114503 (2005).
[33]A. Perronace, J. M. Simon, B. Rousseau, and G. Ciccotti, "Flux expressions and NEMD perturbations for models of semi-flexible molecules," Mol. Phys. **99**(13), 1139–1149 (2001).
[34]M. Zhang and F. Müller-Plathe, "Reverse nonequilibrium molecular-dynamics calculation of the Soret coefficient in liquid benzene/cyclohexane mixtures," J. Chem. Phys. **123**(12), 124502 (2005).
[35]W. Köhler and K. I. Morozov, "The Soret effect in liquid mixtures—A review," J. Non-Equilib. Thermodyn. **41**(3), 151–197 (2016).
[36]X. Chen, R. Liang, Y. Wang, Z. Xia, and G. Cui, "A theoretical study of the temperature gradient effect on the Soret coefficient in n-pentane/n-decane mixtures using non-equilibrium molecular dynamics," J. Non-Equilib. Thermodyn. **45**(4), 319–332 (2020).
[37]A. Olivet and L. F. Vega, "Optimized molecular force field for sulfur hexafluoride simulations," J. Chem. Phys. **126**(14), 144502 (2007).
[38]J. Zhong, R. B. Zhao, and S. H. Xu, "Molecular dynamics simulation of the Soret effect on two binary liquid solutions with equimolar *n*-alkane mixtures," ACS Omega **7**(1), 518–527 (2022); "Correction to 'Molecular dynamics simulation of the Soret effect on two binary liquid solutions with equimolar *n*-alkane mixtures'" **7**(21), 18189 (2022).
[39]A. Firoozabadi, *Thermodynamics and Applications in Hydrocarbon Energy Production* (McGraw-Hill Education, New York, 2016).
[40]H. Zhang, Y. Wang, G. Tao, B. Gui, C. Yin, Y. Chai, and G. Que, "Coarse grained molecular mechanics (MM)/molecular dynamics (MD) force field for petroleum chemistry: I. Coarse grained model for alkanes in petroleum," Acta Chim. Sin. **69**(17), 2053–2062 (2011).
[41]G. Chen, G. Krishan, Y. Yang, L. Tang, and B. Mace, "Numerical investigation of synthetic jets driven by thermoacoustic standing waves," Int. J. Heat Mass Transfer **146**, 118859 (2020).
[42]T. Joshi, O. Parkash, and G. Krishan, "Estimation of energy consumption and transportation characteristics for slurry flow through a horizontal straight pipe using computational fluid dynamics," Phys. Fluids **35**(5), 053303 (2023).
[43]J. Zhong, J. B. Adams, and L. G. Hector, Jr., "Molecular dynamics simulations of asperity shear in aluminum," J. Appl. Phys. **94**(7), 4306–4314 (2003).
[44]J. Zhong, R. Shakiba, and J. B. Adams, "Molecular dynamics simulation of severe adhesive wear on a rough aluminum substrate," J. Phys. D: Appl. Phys. **46**(5), 055307 (2013).
[45]W. Hoover, *Computational Statistical Mechanics* (Elsevier, Amsterdam, 1991).
[46]Y. A. Cengel and A. J. Ghajar, *Heat and Mass Transfer: Fundamentals and Applications*, 5th ed. (Mc Graw Hill, New York, 2011).
[47]D. A. de Mezquia, M. M. Bou-Ali, and J. A. Madariaga, "Mass effect on the Soret coefficient in n-alkane mixtures," J. Chem. Phys. **140**(8), 084503 (2014).
[48]J. E. Bear, T. M. Svitkina, and M. Krause, "Antagonism between Ena/VASP proteins and actin filament capping regulates fibroblast motility," Cell **109**(4), 509–521 (2002).
[49]J. Zhong, L. G. Hector, Jr., and J. B. Adams, "Dynamic decomposition of aliphatic molecules on Al (111) from *ab initio* molecular dynamics," Phys. Rev. B **79**(12), 125419 (2009).
[50]J. Zhong and J. B. Adams, "Adsorption and decomposition pathways of vinylphosphonic and ethanoic-acids on the Al (111) surface: A density functional analysis," J. Phys. Chem. C **111**(20), 7366–7375 (2007).
[51]F. D. Murnaghan, "The compressibility of media under extreme pressures," Proc. Nat. Acad. Sci. U. S. A. **30**(9), 244–247 (1944).
[52]F. Birch, "Finite elastic strain of cubic crystals," Phys. Rev. **71**(11), 809–824 (1947).
[53]A. Stukowski, "Visualization and analysis of atomistic simulation data with OVITO—the Open visualization tool," Modell. Simul. Mater. Sci. Eng. **18**(1), 015012 (2010).
[54]A. Ben-Naim, *Molecular Theory of Solutions*, 1st ed. (Oxford University Press Inc., New York, 2006).
[55]G. A. Voth, *Coarse-Graining of Condensed Phase and Biomolecular Systems* (CRC Press, New York, 2008).
[56]J. M. Prausnitz, R. N. Lichtenthaler, and E. G. de Azevedo, *Molecular Thermodynamics of Fluid-Phase Equilibria*, 3rd ed. (Prentice Hall, New Jersey, 1999).
[57]J. O. Hirschfelder, C. F. Curtiss, and R. B. Bird, *Molecular Theory of Gases and Liquids*, 2nd ed. (John Wiley & Sons, Inc., New York, 1964).
[58]S. Chapman and T. G. Cowling, *Mathematical Theory of Nonuniform Gases*, 3rd ed. (Cambridge University Press, London, 1970).
[59]G. Dominguez, G. Wilkins, and M. H. Thiemens, "The Soret effect and isotropic fractionation in high-temperature silicate melts," Nature **473**, 70–73 (2011).
[60]F. Huang, P. Chakraborty, C. C. Lundstrom, C. Holmden, J. G. Glessner, S. W. Kieffer, and C. E. Lesher, "Isotope fractionation in silicate melts by thermal diffusion," Nature **464**, 396–401 (2010).
[61]M. Shimizu, J. Matsuoka, H. Kato, M. Nishi, H. Visbal, and K. Nagashima, "Role of partial molar enthalpy of oxides on Soret effect in high temperature $CaO\text{-}SiO_2$ melts," Sci. Rep. **8**, 15489 (2018).
[62]D. J. Lacks, G. Goel, C. J. Bopp, J. A. van Orman, and J. A. Lesher, "Isotope fractionation by thermal diffusion in silicate melts," Phys. Rev. Lett. **108**(6), 065901 (2012).
[63]D. C. Montgomery, *Design and Analysis of Experiments*, 10th ed. (Wiley, New York, 2020).
[64]A. Leaty-Dios and A. Firoozabadi, "Molecular and thermal diffusion coefficients of alkane–alkane and alkane–aromatic binary mixtures: Effect of shape and size of molecules," J. Phys. Chem. B **111**(1), 191–198 (2007).

08 April 2024 04:03:49

Published under an exclusive license by AIP Publishing